



Contents lists available at ScienceDirect

Spectrochimica Acta Part A: Molecular and Biomolecular Spectroscopy

journal homepage: www.elsevier.com/locate/saa

Optoelectronic and charge transport properties of D-n-A type 1,3,5-triazine derivatives: A combined experimental and DFT study

Vidya V. M.^a, Someshwar Pola^b, Prabhakar Chetti^{a,*}^a Department of Chemistry, National Institute of Technology, Kurukshetra 136119, Haryana, India^b Department of Chemistry, Osmania University, Hyderabad 500007, Telangana, India

ARTICLE INFO

Article history:

Received 18 March 2020

Received in revised form 28 August 2020

Accepted 7 September 2020

Available online 12 September 2020

Keywords:

Organic optoelectronics

1,3,5-Triazine

 π -Deficient system

First hyperpolarizability

Hole/electron reorganization energy

Electron affinity

Ionization potential

ABSTRACT

The synthesis of five D-n-A type star-shaped octupolar molecules is presented in the current work. The exploration of the potential applicability of molecules under study in organic optoelectronics as electron or hole transporting materials is carried out by DFT methods. All the molecules have a 1,3,5-triazine core, which acts as an electron acceptor (A). Phenyl ring and pyridine ring act as electron donors (D) in AZ and PZ series of molecules respectively. The donor and acceptor core are connected by -NH bridge (n). The crystal structure of a molecule in the PZ series is elucidated. Thermogravimetric studies are carried out to confirm the thermal stability of molecules. The frontier molecular orbitals of molecules are characterized with the help of cyclic voltammetry. With the assistance of DFT methodologies, the whole research presented in this work focuses on the electronic excitations, reorganization energies, electron affinity, ionization potential and features of frontier molecular orbitals of molecules. The investigation of the variation of optoelectronic properties of molecules with changing patterns of nucleophilic substitution on 1,3,5-triazine core and presence of a hetero (nitrogen) atom in the donor part of the molecule is also accomplished.

© 2020 Elsevier B.V. All rights reserved.

1. Introduction

The design and development of novel materials for technological applications have always attracted the attention of people working in the area of organic optoelectronics. Though inorganic materials are leading the field of optoelectronics [1–3]; organic materials are increasingly gaining popularity in the last 20 years because of improvements in the design of materials and methods of purification due to which a significant enhancement in material performance is achieved [4]. Presently, organic materials find applications in organic thin-film-transistors, solar cells, photorefractive devices, light-emitting devices, organic semiconductors, sensors [4] as well as in non-linear optics (NLO) [5–7]. NLO materials and technologies associated with it have generated countless applications such as communication of information, generation of new frequencies of coherent light, generation of ultrashort pulses of light, optical data storage and information processing [8].

1,3,5-triazine is an interesting class of organic heteroaromatic compounds, which are popularly employed in design and applications of organic materials such as charge transport materials [9–11], construction of organic light-emitting materials [12,13] and in the architecture of organic materials, which exhibit non-linear optical (NLO) behavior [14–17]. 1,3,5-Triazine based molecules, metal complexes and materials

find their application in catalysis [18], adsorption of CO₂ gas [19] and in designing of photochromic complexes [20] also.

The idea of consideration of 1,3,5-triazine in building optoelectronic materials comes from the π -deficient nature of triazine ring (and hence can be utilized as an electron acceptor in the molecular backbone), which resulted from the partial localization of π -electrons on the nitrogen atoms in the ring while the carbon atoms of the ring have a lesser amount of electronic charge. And also, because of this the positions 2,4 and 6 of triazine ring are prone to nucleophilic attack by suitable nucleophiles, which facilitates synthetic strategies of 1,3,5-triazine derivatives.

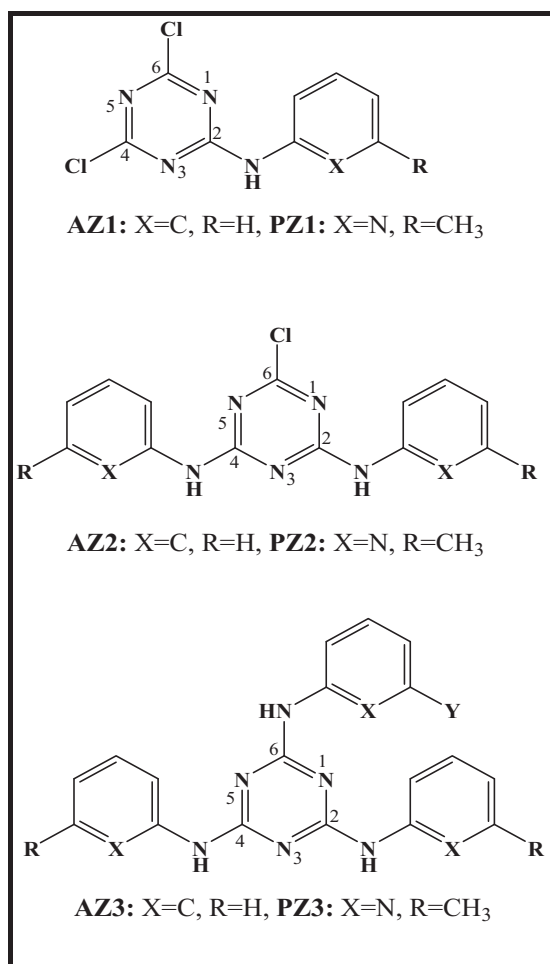
In the recent past, there has been a continuous exploration of the design and synthesis of 1,3,5-triazines and their derivatives [21–27] due to their intriguing features like molecular symmetry and electronic characteristics, which contribute profusely to the ever-proliferating area of optoelectronics.

Keeping all the above facts in mind, we have designed and synthesized few 1,3,5-triazine derivatives (as shown in Scheme 1), which are included in two series namely, AZ and PZ series. Phenyl and pyridine moieties serve as electron donors in AZ and PZ series respectively, while the electron acceptor (1,3,5-triazine) remains the same in both the series.

AZ series contains three molecules; AZ1 (one phenyl ring substituted at position 2 of triazine core via a -NH bridge), AZ2 (two phenyl rings substituted at position 2 and 4 of triazine core each via a -NH bridge)

* Corresponding author.

E-mail address: chetty_prabhakar@yahoo.com (P. Chetti).



Scheme 1. The molecules under investigation.

and AZ3 (three phenyl rings substituted at position 2, 4 and 6 of triazine core each via a -NH bridge). Similarly, PZ series also contains three molecules; PZ1, PZ2 and PZ3, where pyridine moiety is present instead of the phenyl ring. The molecule PZ3 could not be synthesized for the reasons explained in synthesis Section 2.3, but it has been included in computational studies.

The entire work focuses on the electronic excitations, NLO properties, reorganization energies, traits of electron affinity and ionization potential, features and energies of frontier molecular orbitals of molecules under study and how they get manipulated by two factors: 1) increasing nucleophilic substitution on 1,3,5-triazine core in AZ and PZ series and 2) the presence of a hetero (nitrogen) atom in donor part of a molecule, for example, PZ1 has pyridine moiety as compared to AZ1, which has a phenyl moiety.

This work adds to current knowledge of the ever-renewing field of optoelectronics, which requires several novel materials to update itself to fulfill the necessities of information technology and industries and hopes to provide important insights for future architecture and synthesis of optoelectronic materials.

2. Methods

2.1. General experimental methods

All the chemicals are procured from commercial vendors and are used as received. Cyanuric chloride, aniline and K₂CO₃ are purchased

from Avra chemicals. 2-Amino-6-methylpyridine is obtained from Sigma-Aldrich. The AR grade THF and toluene are purchased from Finar chemicals and are used as received. The aluminium TLC plates having TLC Silica gel 60 F₂₅₄ purchased from Merck are used. Column chromatography was done by using silica gel (60-120 Mesh) purchased from LobaChemie. The melting points of samples are measured by the capillary method with the help of NAVYUG melting point device. The finely powdered sample is filled carefully in a capillary tube and inserted in a slot in the device. Thermometer is inserted in another slot and the heating is started in the device. The range of temperature from initiation of melting of sample to complete melting is visually observed and noted. The absorption spectra are measured using EVOLUTION 201 UV-Visible spectrophotometer from Thermo Scientific using a quartz cell of 1 cm path length. IR spectra of products are recorded using IRAffinity-1S spectrophotometer from SHIMADZU. NMR spectra are recorded on BrukerAvance Neo (500 MHz) and Varian (400 MHz) instruments. Mass spectra are recorded using XEVO G2-XS QTOF instrument. A PC controlled CHI 62C electrochemical analyzer was used for cyclic voltammetry studies (solvent: chloroform, scan rate: 100 mV/s) by taking a supporting electrolyte (0.1 M tetrabutylammonium perchlorate). The platinum wire and glassy carbon are employed as counter and working electrodes while considering standard calomel electrode as a reference electrode (the potential of which is calibrated by adopting ferrocene as internal standard) and all the potentials are measured against standard calomel electrode. TGA experiments are carried out on TG Q500 instrument with purging argon at the rate of 10 mL/min and by heating samples at the rate of 10 °C/min. The crystal data was obtained using Bruker D8 Quest PHOTON II diffractometer with monochromatic Mo K α radiation ($\lambda = 0.71073 \text{ \AA}$) at 296 (2) K by using ω and ϕ scan.

2.2. DFT methods

The DFT studies of all molecules in both PZ series (PZ1, PZ2 and PZ3) and AZ series (AZ1, AZ2 and AZ3) are carried out by using Gaussian 16W package [28]. Molecules underwent ground state structure optimization by using B3LYP functional with a 6-31G(d,p) basis set. The potential energy surface showed the presence of local minima, which confirmed that the molecule is stable and has non-negative frequencies.

B3LYP functional is used to predict the properties of the molecules under study since it is known to predict the properties of small organic molecules very well. B3LYP is a hybrid functional, which includes Becke's three-parameter exchange functional (B3) with the non-local correlation functional by Lee, Yang and Parr (LYP) [29,30]. All the calculations are performed by using the B3LYP/6-31G(d,p) method.

The absorption properties of AZ and PZ series of molecules are calculated by TD-B3LYP/6-31G(d,p) method, which are applied on B3LYP/6-31G(d,p) optimized geometries. The first hyperpolarizabilities of all the molecules are computed by the CPHF method [31–33] utilizing the B3LYP/6-31G(d,p) method implemented in the Gaussian 16W package. From the computed tensor components the total first hyperpolarizability (β) is calculated for respective molecules by Eq. (1).

$$\beta = \left(\sum_{ijk} \beta_{ijk}^2 \right)^{1/2} \dots \dots \quad (1)$$

The reorganization energies for all the molecules are calculated at the B3LYP/6-31G(d,p) level. As per the Marcus theory, the charge transfer rate can be expressed as shown in Eq. (2) [34,35].

$$K = \left(\frac{V^2}{h} \right) \left(\frac{\pi}{\lambda T k_B} \right)^{1/2} \exp \left(\frac{-\lambda}{4 T k_B} \right) \dots \quad (2)$$

In Eq. (2), k_B , T, λ and V are the Boltzmann constant, absolute temperature, reorganization energy and intermolecular charge transfer

integral respectively. Eq. (2) suggests that the charge transfer rate mainly depends on values of λ and V . λ is composed of internal and external reorganization energies, whose parameters are influenced by intramolecular vibrations and surrounding medium consecutively. The values of external λ are comparatively lower than those of internal λ [36]. Hence, we have calculated internal λ [total internal hole reorganization energy (λ_h) and electron reorganization energy (λ_e)] by using Eqs. (3) and (4) respectively.

$$\lambda_h = \lambda_1 + \lambda_2 \quad (3)$$

$$\lambda_e = \lambda_3 + \lambda_4 \quad (4)$$

where

$$\lambda_1 = E^+(G_0) - E^+(G_+)$$

$$\lambda_2 = E^0(G_+) - E^0(G_0)$$

$$\lambda_3 = E^-(G_0) - E^-(G_-)$$

$$\lambda_4 = E^0(G_-) - E^0(G_0)$$

In the above equations, where $E^0(G_0)$ is the energy of the neutral molecule in neutral geometry, $E^{+/-}(G_{+/-})$ is the energy of ion (cation/anion) in ionic geometry, $E^{+/-}(G_0)$ is the energy of ion (cation/anion) in neutral geometry and $E^0(G_{+/-})$ is the energy of the neutral molecule in ionic geometry. Here hole and electron are represented by subscripts h and e .

2.3. Synthesis and characterization

The molecules under investigation are presented in Scheme 1. The synthetic protocols of PZ and AZ series of molecules are shown in Figs. 1 and 2 respectively. The synthetic strategies follow simple nucleophilic substitution reactions in the presence of a suitable base, solvent and temperature, which are reported in previous literature [37–44] and are carried out with slight modifications.

In the AZ series, the synthesis proceeded from mono- to di- to tri-substitution without any difficulty by increasing the temperature of reaction as shown in Fig. 2. But in the case of PZ series, mono- and di-substitution occurred readily, while the third substitution was prevented at position 6 of 1,3,5-triazine due to the increased electron density at carbon present in the position 6 (due to electron donation by already substituted two pyridine rings), which is no longer can be attacked by nucleophiles. Though trisubstitution is attempted by means of varying temperature of reaction from room temperature to refluxing temperatures in tetrahydrofuran for extended time scale (24–36 h), the disubstituted molecule remained inert to trisubstitution. The detailed procedures are described in the following discussion. The characterization data (^1H NMR, ^{13}C NMR, Mass and IR spectra) of PZ1, PZ2, AZ1, AZ2 and AZ3 are provided in Figs. S1–S20 (supporting information).

2.3.1. PZ1:4,6-dichloro- N^2 -(6-methyl-2-pyridinyl)-1,3,5-triazine-2-amine

The mixture of cyanuric chloride (0.5 g, 2.71 mmol) and DIPEA (0.3 mL, 2.71 mmol) in 25 mL THF was cooled to 0 °C under N_2 atmosphere. The previously cooled (0 °C) solution of 2-amino-6-methyl pyridine in 25 mL THF was added dropwise to the above reaction mixture over a period of 15 min and stirred for 2 h under N_2 . The reaction was continued to stir at 0–5 °C till all the amine gets exhausted as indicated by TLC. Then, THF was removed from the reaction mixture under reduced pressure. Further, the reaction mixture was extracted in ethyl acetate (3×30 mL) and the organic layer was dried over anhydrous Na_2SO_4 , filtered and the solvent was evaporated under reduced pressure to obtain a white residue. The residue is purified by silica column chromatography (ethyl acetate/hexane: 1:8→1:7) to get a white solid (0.562 g, 81% yield). M.P: 132–135 °C. IR (KBr): 3234 cm^{-1} (medium, -NH), 2924 cm^{-1} (medium, -CH₃), 1606 cm^{-1} (medium, -C=N-), 1250 cm^{-1} (strong, -CH₃). ^1H NMR (500 MHz, CDCl_3): δ 9.47 (br s, 1H, NH), 8.06 (m, $J = 5$ Hz, 1H, ArH), 7.70 (t, $J = 5$ Hz, 1H, ArH), 6.99 (d, $J = 5$ Hz, 1H, ArH), 2.52 (s, 3H, CH₃). ^{13}C NMR (500 MHz, CDCl_3): δ 163.66, 157.71, 149.26, 138.86, 120.17, 111.93, 23.80. EI-MS: Calculated for $\text{C}_9\text{H}_7\text{Cl}_2\text{N}_5$ is 255.01, found 255.82 (M^+).

2.3.2. PZ2:6-chloro- N^2, N^4 -bis-(6-methyl-2-pyridinyl)-1,3,5-triazine-2,4-diamine

Cyanuric chloride (1 g, 5.42 mmol) was dissolved in 30 mL of THF in a 100 mL round bottom flask and was added with DIPEA (~2 mL, 11.38 mmol) under N_2 atmosphere at room temperature. Then 2-amino-6-methyl pyridine (1.23 g, 11.38 mmol) was dissolved in 30 mL of THF and added dropwise to the above reaction mixture over a period of 30 min. The reaction mixture was stirred at rt. under nitrogen for 8 h. The progress of the reaction was monitored by TLC. Then THF was stripped off from reaction mixture by rotavaporization followed by extraction of product in ethyl acetate (3×50 mL). The organic layer was dried over anhydrous Na_2SO_4 , filtered and was concentrated under reduced pressure to obtain a red-colored residue. The residue was purified by using column chromatography using silica gel (ethyl acetate/hexane: 1:5→1:4) to obtain pale yellow solid (1.29 g, 73% yield). M.P: 165–170 °C. IR (KBr): 3232 cm^{-1} –3116 cm^{-1} (br, medium, -NH), 2924 cm^{-1} (medium, -CH₃), 1737 cm^{-1} (medium, -C=N), 1273 cm^{-1} (strong, -CH₃). ^1H NMR (500 MHz, CDCl_3): δ 8.03 (br s, 2H, ArH), 7.56 (br s, 2H, ArH), 6.85 (d, $J = 10$ Hz, 2H, ArH), 2.45 (s, 6H, CH₃). ^{13}C NMR (500 MHz, CDCl_3): δ 169.91, 163.59, 157.22, 150.49, 138.29, 118.79, 111.50, 23.88. ESI-MS: Calculated for $\text{C}_{15}\text{H}_{14}\text{ClN}_7$ is 327.10, found 328.07 ($\text{M} + \text{H}^+$).

2.3.3. AZ1:4,6-dichloro- N -phenyl-1,3,5-triazine-2-amine

The mixture of cyanuric chloride (1 g, 5.42 mmol) and K_2CO_3 (0.75 g, 5.42 mmol) were taken in a 100 mL rb containing 30 mL toluene and were cooled to 0° C. To this reaction mixture, a previously cooled (0° C) solution of aniline (~0.5 mL, 5.42 mmol) in 20 mL of toluene was added dropwise over a period of 15 min. Further, the reaction was stirred at 0–5 °C for 2 h to obtain a white precipitate and until all aniline gets exhausted as indicated by TLC. Toluene was removed from the reaction mixture under reduced pressure. The product was extracted in

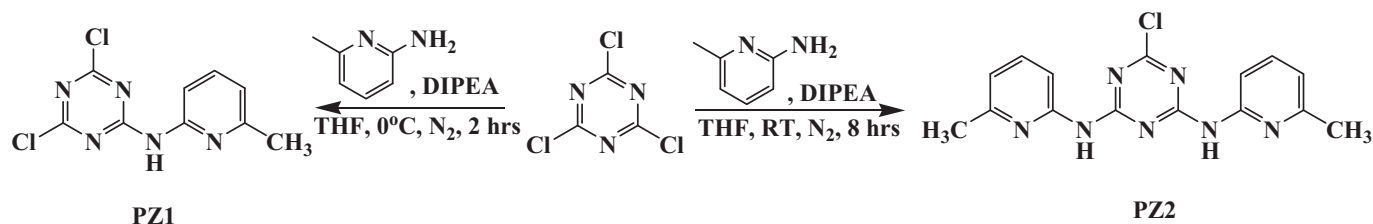


Fig. 1. The synthetic pathway of PZ1 and PZ2.

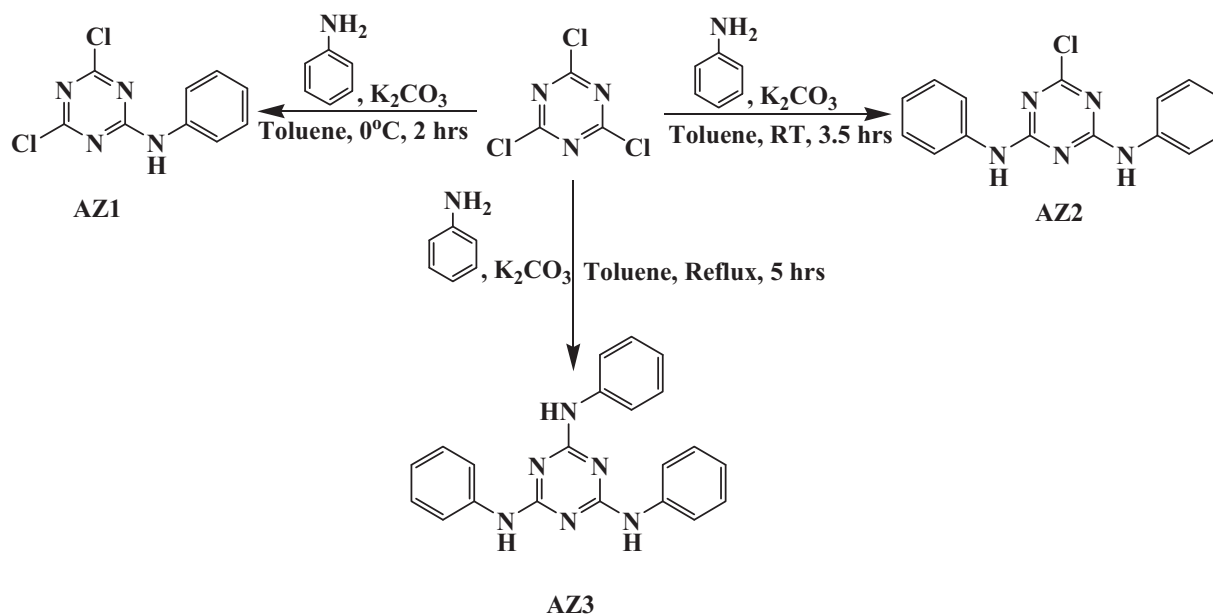


Fig. 2. The synthetic pathway of AZ1, AZ2 and AZ3.

CHCl₃ (3×50 mL), the organic portion was dried over anhydrous Na₂SO₄, filtered and the solvent was stripped off by rotavaporizing to obtain a white residue. The residue was purified by silica column chromatography (ethyl acetate/hexane: 1:15→1:12) to obtain a white solid (0.87 g, 66% yield). Colorless crystals (ethyl acetate/hexane: 1:15). M.P: 125–128 °C. IR (KBr): 3369 cm⁻¹ (medium, -NH), 1620 cm⁻¹ (medium, -C=N-). ¹H NMR (500 MHz, CDCl₃): δ 7.80 (br s, 1H, NH), 7.54 (d, J = 5 Hz, 2H, ArH), 7.40 (t, J = 10 Hz, 2H, ArH), 7.22 (m, 1H, ArH). ¹³C NMR (500 MHz, CDCl₃): δ 171.38, 170.19, 164.12, 135.70, 129.31, 125.91, 121.44. ESI-MS: Calculated for C₉H₆Cl₂N₄ is 240.00, found 241.01 (M + H)⁺.

2.3.4. AZ2: 6-chloro-N²,N⁴-diphenyl-1,3,5-triazine-2,4-diamine

A 100 mL rb was charged with cyanuric chloride (0.5 g, 2.71 mmol) and K₂CO₃ (0.786 g, 5.69 mmol) and was added with 30 mL of toluene at rt. A solution of aniline (0.5 mL, 5.69 mmol) in 20 mL of toluene was added dropwise to the above reaction mixture over a period of 30 min. The reaction was stirred at rt. for 3.5 h till the spot of aniline disappears in TLC. Toluene was removed from the reaction mixture by rotavaporizing to get a white residue. The product was extracted in CHCl₃ (3×50 mL), dried the organic layer over anhydrous Na₂SO₄, filtered and concentrated the organic portion under reduced pressure to get a white residue. The residue was purified by column chromatography using silica gel (ethyl acetate/hexane: 1:10→1:8) to obtain a white solid (0.57 g, 70% yield). Colorless crystals (ethyl acetate/hexane: 1:10). M.P: 185–188 °C. IR (KBr): 3265 cm⁻¹ (medium, -NH), 1627 cm⁻¹ (medium, -C=N-). ¹H NMR (500 MHz, CDCl₃): δ 7.70 (br s, 2H, NH), 7.53 (d, J = 10 Hz, 4H, ArH), 7.34 (t, J = 10 Hz, 4H, ArH), 7.15 (t, J = 10 Hz, 2H, ArH). ¹³C NMR (MHz, CDCl₃): δ 164.25, 137.15, 128.93, 124.68, 121.57. ESI-MS: Calculated for C₁₅H₁₂ClN₅ is 297.08, found 298.10 (M + H)⁺.

2.3.5. AZ3: N²,N⁴,N⁶-Triphenyl-1,3,5-triazine-2,4,6-triamine

Cyanuric chloride (1 g, 5.42 mmol) was dissolved in 50 mL of toluene followed by the addition of K₂CO₃ (2.32 g, 16.80 mmol) and refluxed. To this reaction mixture, aniline (1.5 mL, 16.80 mmol) was added in one portion to observe white precipitate immediately. The reaction mixture was refluxed for 5 h. The progress of the reaction was monitored by TLC. Toluene was stripped off from the reaction mixture by rotavaporizing to obtain a white residue. The crude product was extracted in CHCl₃

(3×50 mL). The organic layer was dried over anhydrous Na₂SO₄, filtered and the solvent was concentrated under reduced pressure. The residue was purified by silica gel column chromatography (ethyl acetate/hexane: 1:6→1:4) to obtain a white solid (1.65 g, 86% yield). M.P: 227–230 °C. IR (KBr): 3406 cm⁻¹ (medium, -NH), 1614 cm⁻¹ (medium, -C=N-). ¹H NMR (500 MHz, CDCl₃): δ 7.59 (d, J = 10 Hz, 6H, ArH), 7.35 (t, J = 10 Hz, 6H, ArH), 7.16 (br s, 1H, NH), 7.11 (m, 3H, ArH), 1.78 (br s, 1H, NH). ¹³C NMR (MHz, CDCl₃): δ 164.48, 138.47, 128.81, 123.45, 120.84. ESI-MS: Calculated for C₂₁H₁₈N₆ is 354.16, found 355.13 (M + H)⁺.

3. Results and discussion

3.1. Crystal structure

The co-crystallization of organic molecules with inorganic salts is known in past literature [45,46]. We also came across co-crystallization of PZ2 with copper chloride during attempts to form complexes of PZ2 with metal salts (the crystals of pure PZ2 are very weak to be analyzed by single-crystal analysis technique). Yellow-colored co-crystals are formed under the following conditions. 10 mL of CH₃CN:CHCl₃ (5:1) was added with PZ2 (1 mol), CuCl₂(1/3 mol) and few drops of HCOOH and kept at 60 °C in an oven for 3 days. A suitable yellow-colored single crystal was carefully chosen under a polarizing microscope and stuck to a very fine glass fiber with the help of cyanoacrylate (super glue) adhesive. The single-crystal X-ray diffraction data were collected with Bruker D8 Quest PHOTON II diffractometer with monochromatic Mo Kα radiation (λ = 0.71073 Å) at 296 (2) K by using ω and φ scan. The X-ray generator was operated at 50 kV and 20 mA. The data were reduced by using APEX3. The diffraction profiles integration was done with SAINTPLUS [47] program and absorption correction (multiscan) has been done by SADABS program [48]. The structure was solved and refined using SHELXL97 program [49] existing in the WinGx suite of programs (version 1.63.04a) [50]. All the hydrogen positions were initially located in the difference Fourier maps and the hydrogen atoms were placed in geometrically ideal positions and refined in the riding mode. The final refinement included atomic positions of all the atoms, isotropic thermal parameters for all the hydrogen atoms and anisotropic thermal parameters for all the non-hydrogen

Table 1

Crystal data and structure refinement parameters for co-crystal of PZ2 with copper chloride.

Empirical formula	C ₆₀ H ₅₆ Cl ₁₆ Cu ₃ N ₂₈
Formula weight	1927.15
Crystal system	Orthorhombic
Space group	<i>Fdd</i> (No.70)
<i>a</i> (Å)	17.8315(15)
<i>b</i> (Å)	25.607(2)
<i>c</i> (Å)	32.449(3)
α (°)	90.00
β (°)	90.00
γ (°)	90.00
<i>V</i> (Å ³)	14,816(2)
<i>Z</i>	8
<i>D</i> (calc/gcm ⁻³)	1.728
μ (mm ⁻¹)	1.494
λ (Mo K α /Å)	0.71073
θ range (°)	3.05–25.00
Total data collected	35,590
Unique data	3171
Rint	0.0457
R indexes [<i>I</i> > 2 σ (<i>I</i>)]	R ₁ = 0.0731; wR ₂ = 0.2118
R indexes (all data)	R ₁ = 0.0901; wR ₂ = 0.2297

$$R1 = \frac{\sum ||F_o| - |F_c||}{\sum |F_o|}; wR2 = \frac{[\sum [w(F_o^2 - F_c^2)^2] / \sum [w(F_o^2)^2]]^{1/2}}{\sum [w(F_o^2)^2 + (aP)^2 + bP]}; P = [\max(F_o, 0) + 2(F_c)^2] / 3.$$

atoms. The detailed description of the crystal structure solution and final refinement parameters for the structure is given in Table 1.

The X-ray single crystallography confirmed the crystallization in the orthorhombic crystal system with space group *Fdd*. The asymmetric unit of the resultant crystal structure contains two copper chloride moieties with the target molecule. The asymmetric unit is represented as Fig. 3. All three aromatic rings connected via N-atom are on the same plane. The present structure is stabilized by hydrogen bonding interactions between corresponding atoms N4—H4···Cl03 and N7—H7B···Cl1. The detailed information about hydrogen bonding is provided in Table S1. Hydrogen bonding interactions between the atoms have been calculated by PLATON [51].

The crystallographic data for the compound can be found in CCDC No: 1968199 by free of charge from The Cambridge Crystallographic Data Centre (CCDC) via www.ccdc.cam.ac.uk/data_request/cif.

Since the crystal structure of only one molecule (PZ2) is obtained we took the help of DFT methods to understand the structure and geometry of all molecules under study. For this, the molecules are optimized in their ground state by B3LYP/6-31G (d, p) method. The crystal structure of AZ1 is experimentally known [52]. The experimental geometrical parameters of AZ1 and PZ2 are compared with their theoretical

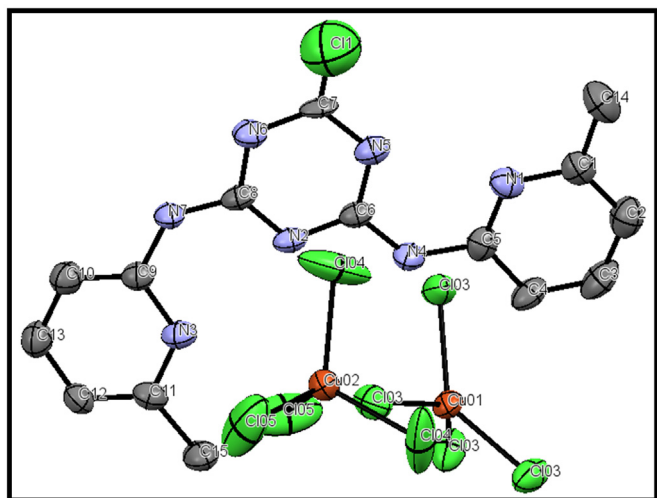


Fig. 3. Ortep diagram of the compound PZ2. All the hydrogen atoms are omitted for clarity.

geometrical parameters (Table S2A and S2B respectively, supporting information) to reveal that the B3LYP/6-31G (d, p) method calculated molecular geometries are agreeing very well with the experimental observations. Hence the B3LYP/6-31G (d, p) method is applied for all molecules for ground state geometry optimization. The ground state geometries of two representative molecules AZ2 and PZ2 are shown in Fig. 4 and those of AZ1, AZ3, PZ1 and PZ3 are provided in Fig. S21. From Figs. 4 and S21, it appears that all the molecules are planar with dihedral angles between central triazine core and the substituted aromatic rings (phenyl/pyridine in the case of AZ/PZ series) being less than 5°.

The sp³ geometry around nitrogen atom present in the nitrogen bridge between triazine core and substituted aromatic rings has given rise to various configurations of molecules, which arise mainly due to N (from nitrogen bridge) – C (from aromatic ring) bond rotation. The configurations of molecules (except AZ1, since it does not show any other configuration) falling within 7 kcal/mol relative energy range are shown in Fig. 5. It is also noticeable that the molecule PZ2 crystallizes in configuration PZ2A in the solid state. The configuration PZ2A has 0.002 kcal/mol relative energy as compared to PZ2.

3.2. Absorption properties

The absorption spectra of synthesized molecules (PZ1, PZ2, AZ1, AZ2 and AZ3) are recorded in CHCl₃ at 1 × 10⁻⁶ M concentration and at room temperature. The experimental absorption spectra and UV data are presented in Fig. 6 and Table 2 respectively. Also, the TD-B3LYP/6-31G (d, p) calculated wavelength of maximum absorption (λ_{cal}), oscillator strength (*f*), major electronic transitions and mixing co-efficients (%C_i) of all molecules are provided in Table 3. The theoretical absorption spectra of AZ and PZ series of molecules are shown in Figs. S22A and S22B respectively.

In spite of varied substitutions, the common feature of absorption spectra of molecules AZ1, AZ2, AZ3, PZ1 and PZ2 is the presence of two absorption systems (namely I and II) [53] as seen in Fig. 6. The absorption system I is centered at ~245 nm (which is not visible completely because of the cut-off wavelength of CHCl₃ being around 240–250 nm) while absorption system II is centered at ~275 nm. The broad bands observed in absorption system II is the result of multiple electronic transitions occurring in the triazine moiety [54]. Also, the broadness of UV spectra of triazines can be related to the prominent vibrational frequencies present in s-triazine n→π* transitions as assigned by Brinen et al. [55].

The absorption system I show the absorption band at approximately 245 nm for each molecule, which is attributed to the (short wavelength and high energy) π→π* electronic transition (since this band did not show any shift in absorption maxima with changing solvent polarity) as investigated by Hirt et al. [56]. This observation is consistent with the UV spectra of benzene and other nitrogen heterocycles [57]. In order to gain more insight into the electronic transitions in absorption system I, the TD-DFT calculations for first ten excited states of molecules are carried out and the results are presented in Table 3. From Table 3, it is confirmed that the band in the absorption system I arise as a result of several electronic transitions occurring in excited states other than S1 and S2. In molecule PZ1, the absorption system I is comprised of major electronic transitions HOMO→LUMO+2, HOMO-4→LUMO and HOMO-1→LUMO with absorption wavelengths of 246 nm (in S3), 246 nm (in S4) and 235 nm (in S5) respectively. The molecule PZ2 evidences the major electronic transition HOMO→LUMO+2 (in S5) with absorption wavelength 251 nm, which is included in absorption system I. The absorption system I in molecule AZ1 is constituted of major electronic transitions HOMO-1→LUMO (in S3), HOMO-3→LUMO (in S4) and HOMO-2→LUMO+1 (in S5) with absorption wavelengths of 250 nm, 245 nm and 233 nm respectively. Similarly, the major electronic transitions occurring in absorption system I of molecules AZ2 and AZ3 are mentioned in Table 3.

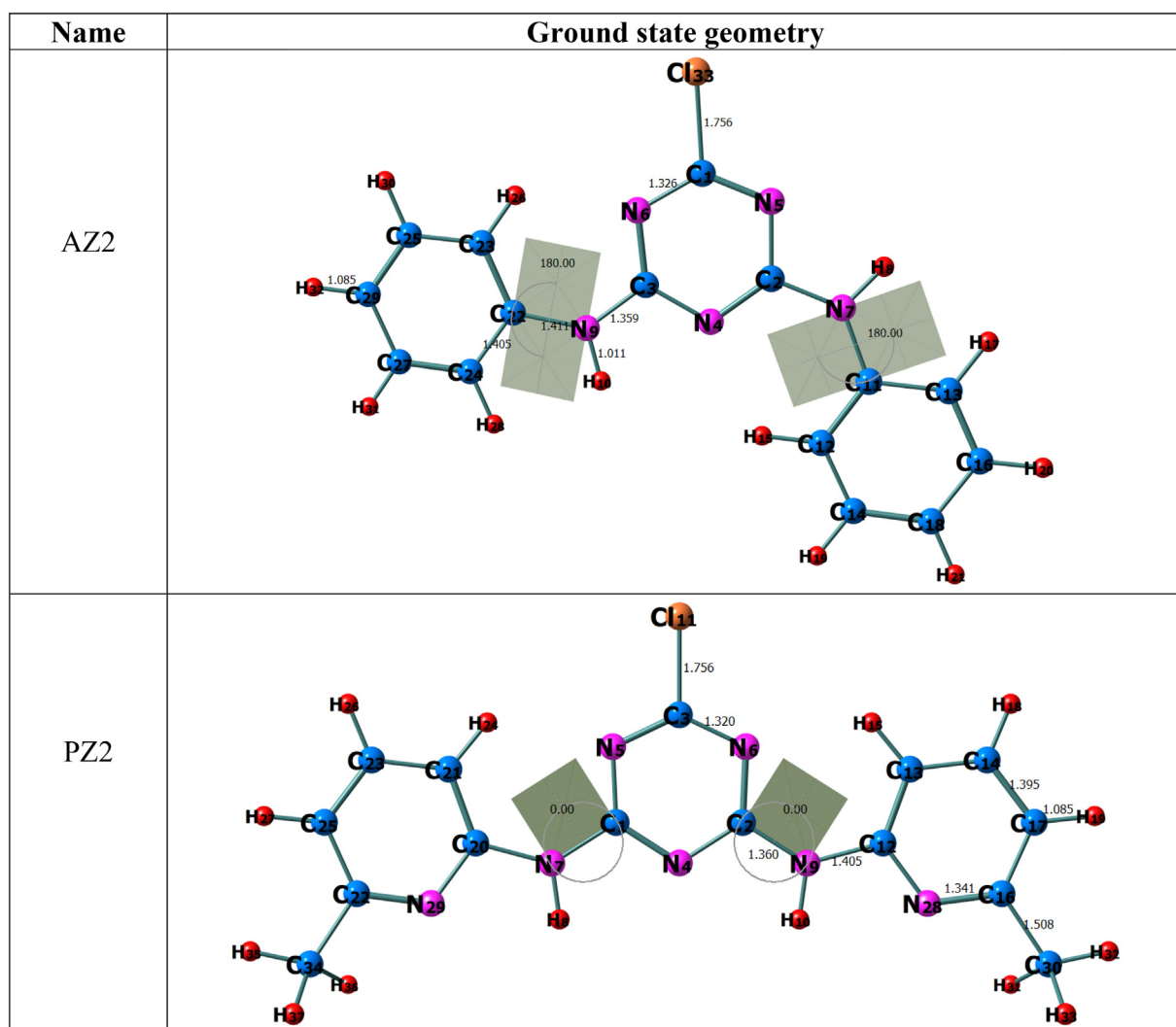


Fig. 4. The optimized ground state geometries of AZ2 and PZ2 calculated at B3LYP/6-31G (d, p) level of theory.

The absorption system II consists of a broad band centered at nearly 275 nm, which is assigned by Brealey et al. [58] to be the outcome of promotion of a non-bonding (n) lone pair nitrogen electron (having σ -symmetry) to a π^* (antibonding) orbital. The discussion on the absorption system II takes an important input from the work of Innes and co-workers [59], who assigned the long-wavelength band in azines to be originating from $n \rightarrow \pi^*$ electronic transitions. This $n \rightarrow \pi^*$ forbidden electronic transition is also noted by Halverson et al. [57], who observed clear solvent shift characteristics of this transition involving non-bonding electrons. This absorption system II consists of four $n \rightarrow \pi^*$ electronic transitions out of which three are forbidden and one is allowed as suggested by Goodman et al. [54] for s-triazines. The UV spectra of compounds AZ1, AZ2, AZ3, PZ1 and PZ2 (which belong to azine class of molecules) show few weak features in absorption system II, which may be the result of previously cited four $n \rightarrow \pi^*$ electronic transitions, whose intensity is increased due to reduction of symmetry around triazine nucleus (because of varied substitutions on triazine core), which has caused increased dipole strength and hence has increased transition probability [60].

In order to obtain a clear comprehension of the multiple electronic transitions, which have convoluted in absorption system II, the deconvolution of the experimental UV spectrum of one representative molecule AZ1 is carried out and is shown in Fig. 7.

The deconvoluted UV spectrum of AZ1 is constituted of five major curves/electronic transitions, which are represented by five elements. A very intense peak in the absorption system I is the result of $\pi \rightarrow \pi^*$ transition as discussed above and is represented by element 1. In agreement with the report by Goodman [54], one allowed $n \rightarrow \pi^*$ transition (represented by element 2, higher intensity peak) and three forbidden $n \rightarrow \pi^*$ transitions (represented by element 3 - element 5, lower intensity peaks) are observed in absorption system II. Similar type of transitions can be expected in molecules AZ2, AZ3, PZ1 and PZ2, since they all show similar absorption features and all bear a triazine nucleus. Further, to get more understanding of electronic transitions occurring in absorption system II, the help of results of TD-DFT calculations, which are shown in Table 3 is taken. The major electronic transitions responsible for the occurrence of element 2 can be assigned as HOMO \rightarrow LUMO+1 (with 271 nm in S2), HOMO-1 \rightarrow LUMO (274 nm in S3), HOMO \rightarrow LUMO+1 (272 nm in S2), HOMO \rightarrow LUMO+1 (274 nm in S3) and HOMO \rightarrow LUMO+1 (270 nm in S3) in molecules PZ1, PZ2, AZ1, AZ2 and AZ3 respectively (Table 3). Also, the low-intensity absorption bands in element 3, element 4 and element 5 are expected to be originating from the major electronic transitions HOMO \rightarrow LUMO (298 nm in S1), HOMO \rightarrow LUMO+1 (284 nm in S1), HOMO \rightarrow LUMO (311 nm in S1), HOMO-1 \rightarrow LUMO (289 nm in S1) and HOMO \rightarrow LUMO+1 (280 nm in S1) in molecules PZ1, PZ2, AZ1, AZ2 and AZ3 respectively. A

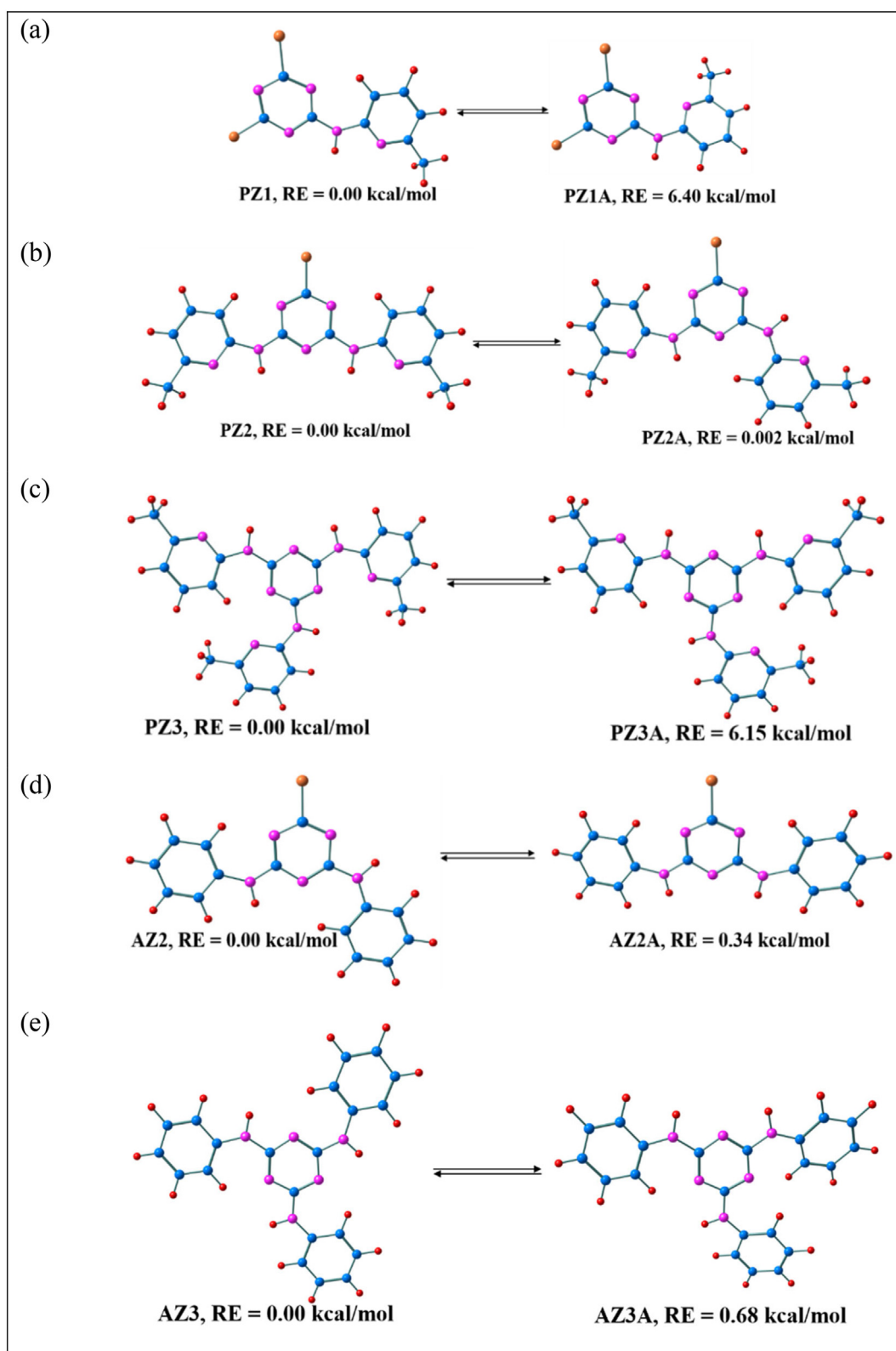


Fig. 5. The configurations of (a) PZ1, (b) PZ2, (c) PZ3, (d) AZ2 and (e) AZ3 having their relative energies within 7 kcal/mol calculated at B3LYP/6-31G (d, p) level of theory.

schematic illustration of major electronic transitions in absorption system II in representative molecules AZ2 and PZ2 is shown in Fig. 8.

From the above discussions, it is evident that TD-DFT calculations follow the trend of experimental results to a fairly good extent.

The absorption features of molecule PZ3 are anticipated to be similar to those of PZ1, PZ2, AZ1, AZ2 and AZ3. The theoretical absorption data and absorption spectrum of PZ3 are included in Table 3 and Fig. S22B respectively.

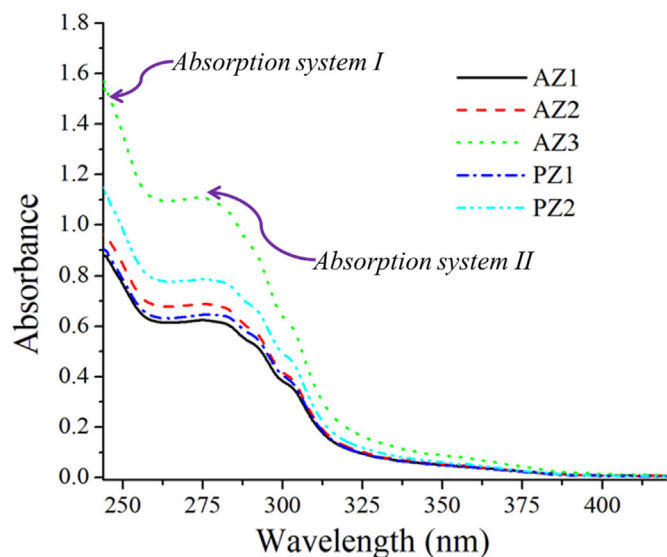


Fig. 6. The absorption spectra of molecules measured at 1×10^{-6} M concentration in CHCl_3 at room temperature.

It appears from Table 2 that neither nucleophilic substitution pattern nor the incorporation of nitrogen atom bears any significant effect on the λ_{max} (which is an allowed $n \rightarrow \pi^*$ transition in absorption system II) of molecules. This trend is also reflected in the high-intensity λ_{cal} values from TD-DFT calculations (Table 3).

But, the low-intensity electronic transitions in excited state S1 (Table 3) seem to be affected by the pattern of nucleophilic substitution such that, a blue shift of 14 nm (22 nm) is observed as we move from PZ1 (AZ1) to PZ2 (AZ2) in accordance with the observation of Hirt et al. [53]. This is perhaps because of the fact that PZ1 (AZ1) is a D-n-A type molecule, where electron delocalization from donor to acceptor occurs without any hindrance and hence, they absorb at higher wavelengths. The system changes to D-n-A-n-D type in the case of PZ2 (AZ2), where electron delocalization is mostly limited from donor end to central acceptor rather than across the whole molecule and hence the absorption wavelength decreases. Further, the absorption wavelength of PZ3 (AZ3) in excited state S1 gets blue-shifted by 10 nm (39 nm) from PZ1 (AZ1).

3.3. Electrochemical properties

The HOMO indicates the energy required for removal of an electron from a molecule, which is an oxidation process and LUMO is the energy needed to add an electron to a molecule, which is a reduction process. Cyclic voltammetry helps in determining the energies of HOMO and LUMO of a molecule by means of measurement of the redox potentials.

The electrochemical behavior of synthesized molecules is characterized by cyclic voltammetry (CV) studies (experimental details are given

Table 2

The experimental absorption maxima (λ_{exp} in nm) in CHCl_3 measured at a concentration of $1 \mu\text{M}$, molar extinction coefficient (ϵ in $\text{L M}^{-1} \text{cm}^{-1}$), melting point (MP in $^\circ\text{C}$) and decomposition temperature (T_d in $^\circ\text{C}$) of molecules AZ1, AZ2, AZ3, PZ1 and PZ2.

Name	λ_{exp}	ϵ	MP	T_d
AZ1	274	0.623×10^6	125–128	132
AZ2	269	0.689×10^6	185–188	205
AZ3	273	1.103×10^6	227–230	295
PZ1	277	0.764×10^6	132–135	158
PZ2	275	1.008×10^6	167–170	245

Table 3

The calculated absorption maxima (λ_{cal} in nm), oscillator strength (f), major electronic transitions (MT) and mixing co-efficient ($\%C_i$) of molecules under study in first five excited states calculated at B3LYP/6-31G (d, p) level of theory.

Name	Excited state	λ_{cal}	f	MT	$\%C_i^a$
PZ1	S1	298	0.006	H→L	98
	S2	271	0.567	H→L + 1	93
	S3	246	0.028	H→L + 2	77
	S4	246	0.005	H→L + 2	70
	S5	235	0.002	H→L + 2	58
PZ2	S1	284	0.288	H→L + 1	66
	S2	282	0.003	H→L	94
	S3	274	0.995	H→L + 1	66
	S4	260	0.054	H→L + 1	72
	S5	251	0.006	H→L + 2	66
PZ3	S1	286	0.011	H→L	71
	S2	281	0.355	H→L + 1	55
	S3	274	0.322	H→L + 1	49
	S4	272	0.730	H→L + 1	48
	S5	263	0.084	H→L + 2	56
AZ1	S1	311	0.004	H→L	98
	S2	272	0.613	H→L + 1	98
	S3	250	0.022	H→L + 1	96
	S4	245	0.005	H→L + 1	92
	S5	233	0.002	H→L + 1	87
AZ2	S1	289	0.026	H→L + 1	65
	S2	282	0.004	H→L	73
	S3	274	1.040	H→L + 1	77
	S4	258	0.222	H→L + 1	80
	S5	250	0.010	H→L + 2	28
AZ3	S1	280	0.122	H→L + 1	34
	S2	276	0.032	H→L	67
	S3	270	0.743	H→L + 1	49
	S4	268	0.727	H→L + 1	40
	S5	266	0.147	H→L + 1	34
				H→L + 1	29

^a Mixing co-efficients above 25% are considered.

in Section 2.1) to obtain information about their frontier molecular orbitals.

The oxidation plateaus obtained from CV measurements (where potential is swept from 0 V to +2 V) are not well defined to calculate accurate oxidation potentials. Hence the reduction part of the cycle (where potential is swept from 0 V to -2 V), which showed well-characterized reduction plateaus is preferred for CV studies. The half-

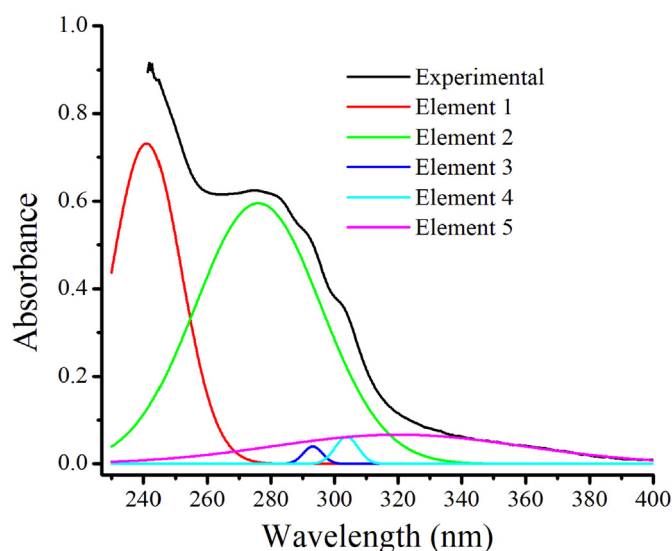


Fig. 7. The deconvoluted UV spectra of molecule AZ1.

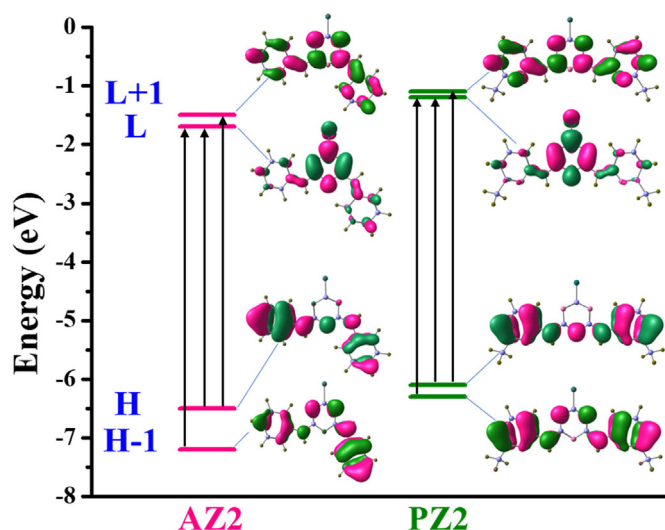


Fig. 8. The major electronic transitions occurring in absorption system II of molecules AZ2 and PZ2 calculated at B3LYP/6-31G (d,p) level of theory.

wave potential ($E_{red}^{1/2}$) in voltammogram [61] is used to calculate LUMO in previous literature [62–65] and the same method is applied in the current work.

In the forward scan, the potential is swept negatively from the starting potential 0 V up to the switching potential -2.0 V. This is denoted as a cathodic trace. Then the direction of the scan is reversed to take a potential sweep from -2.0 V to 0 V (anodic trace). The CV curves of molecules AZ1, AZ2, AZ3, PZ1 and PZ2 are provided in Fig. S23.

The cathodic trace of each molecule shows a minimum one well-defined reduction peak. The three azomethine groups ($-N=C-$) present in the triazine core may be subjected to a reduction in this class (azines) of molecules [66]. But oxidation of these molecules appears to be sluggish since the oxidation peaks in the anodic trace are not as well defined as reduction ones.

The difference between peak potentials of redox couple in each molecule is larger than 57 mV and in no case the ratio anodic peak current (i_{pa})/cathodic peak current (i_{pc}) is equal to 1. Hence, the redox reactions (involving the azomethine group) in each voltammogram presented in Fig. S23 are non-reversible reactions. Also, the deviation of the value of ratio i_{pa}/i_{pc} from unity indicates that many chemical reactions (triggered by electron transfer) such as isomerization, dissociation and association are happening in molecules [67]. These may be the reasons behind the huge asymmetry in curve shapes.

Then LUMO value of all the molecules is calculated from $E_{red}^{1/2}$ value as per Eq. (5) and are shown in Table 4.

$$E_{LUMO} = -[E_{red}^{1/2} + 4.8] \text{ V} \dots \dots \quad (5)$$

Table 4

The electrochemical half-wave potential ($E_{red}^{1/2}$ in V), the energy of LUMO (E_{LUMO} in eV), absorption edge (λ_{edge} in nm), optical band gap (E_g^{opt} in eV) and energy of HOMO (E_{HOMO} in eV) of AZ1, AZ2, AZ3, PZ1 and PZ2.

Molecule	$E_{red}^{1/2}$ ^a	E_{LUMO} ^a	λ_{edge}	E_g^{opt} ^b	E_{HOMO} ^c
AZ1	-1.14	-3.66	400	3.10	-6.76
AZ2	-1.18	-3.62	397	3.12	-6.74
AZ3	-1.32	-3.48	390	3.18	-6.66
PZ1	-1.06	-3.74	396	3.13	-6.87
PZ2	-1.15	-3.65	392	3.16	-6.81

^a $E_{LUMO} = -(E_{red} \text{ w.r.t. Fc/Fc}^+ + 4.8) \text{ eV}$.

^b $E_g^{opt} = \left(\frac{1240}{\lambda_{edge}}\right) \text{ eV}$.

^c $E_{HOMO} = (E_{LUMO} - E_g^{opt}) \text{ eV}$.

In the molecule AZ1, the transfer of three electrons (or three reductions) gives rise to three reduction plateaus (Fig. S23). The molecule AZ1 starts the first reduction at -0.885 V and shows the average $E_{red}^{1/2}$ value of -1.14 V. It is clear from the Table 4, destabilization of LUMO levels with the successive addition of substituent on triazine core.

Optical gap (E_g^{opt}) represents the energy of the lowest electronic transition facilitated by the absorption of a single photon [68]. And hence it involves the electronic transition HOMO→LUMO, which is lowest in energy and highest in wavelength as compared to all other transitions. Hence, in order to calculate the optical gap one can look for an absorption edge in UV spectrum of a molecule. In terms of physics, the absorption edge (λ_{edge}) is indicated at a wavelength at which there is a sudden increase in the degree of absorption of electromagnetic radiation by a substance. The λ_{edge} is associated with the sharply defined energy levels occupied by electrons. Hence it would be useful to estimate the optical gap by using λ_{edge} . A few reports in the recent past have utilized this method for calculating the optical gap [69–72].

The E_g^{opt} is obtained from the UV absorption spectra of molecules [73] by considering λ_{edge} using Eq. (6).

$$E_g^{opt} \text{ (in eV)} = \frac{1240}{\lambda_{edge} \text{ (in nm)}} \dots \dots \quad (6)$$

Then, by using values of E_{LUMO} and E_g^{opt} ; the E_{HOMO} values are calculated by using Eq. (7).

$$E_{HOMO} = (E_{LUMO} - E_g^{opt}) \dots \dots \quad (7)$$

The experimental E_{HOMO} , E_{LUMO} and E_g^{opt} values of all the synthesized molecules are provided in Table 4. The CV data in Table 4 points out that, increasing substitution on triazine core has resulted in the destabilization of both HOMO and LUMO levels of molecules (to different extents). From Table 4, it is clear that the magnitude of destabilization of LUMO of molecules (as substitution increases) is higher than that of their HOMO. This causes the energy gap to increase slightly as the substitution on triazine core increases. The same trend is followed by theoretically calculated HOMO and LUMO levels of molecules (Fig. 9 and Table S3) in AZ and PZ series.

3.4. Thermogravimetric studies

The resistance of a material to undergo decomposition when exposed to higher temperatures makes it thermally stable and increases the probability of material being applicable in the construction of optoelectronic materials. Hence, thermogravimetric (TGA) studies are

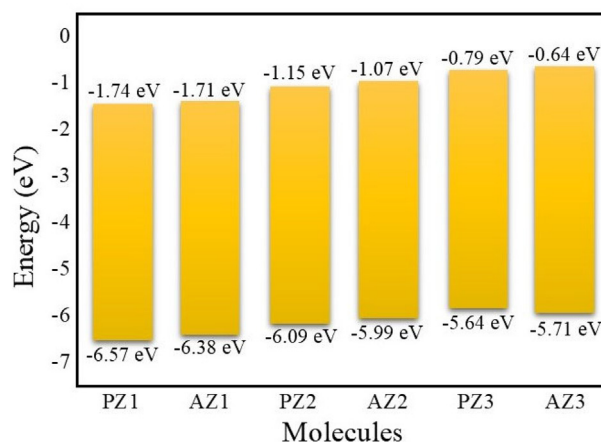


Fig. 9. The schematic comparison of energy levels of HOMO and LUMO of all the molecules under study at B3LYP/6-31G (d, p) level of theory.

conducted on synthesized compounds to evaluate their thermal stability and TGA curves are shown in Fig. S24. The decomposition temperatures (T_d) are provided in Table 2. In AZ series of molecules thermal stability varies in the order: AZ3 > AZ2 > AZ1. In PZ series of molecules PZ1 is more thermally stable than PZ2. The molecules AZ2, AZ3 and PZ1 show higher thermal stability than AZ1 and PZ2 (which show moderate thermal stabilities).

3.5. Frontier molecular orbitals

The frontier molecular orbitals (HOMO and LUMO) of all the molecules are visualized at B3LYP/6-31G (d, p) level of theory and are shown in Fig. S25.

The central triazine core acts as an electron acceptor and the pyridine (phenyl) ring acts as an electron donor in PZ (AZ) series of molecules. The D-n-A type dipolar molecular architecture is observed in molecule PZ1 (AZ1), where electron density flows from pyridine (phenyl) moiety into triazine core entirely leading to the total delocalization of electrons.

The D-n-A-n-D type of molecular design is contained in the molecule PZ2 (AZ2). Here electron density shifts from both donor end into the central triazine ring. Now triazine core has got an increased number of electron donors, but its capacity to attract electrons has not increased and hence it cannot accept all the electrons and hence some amount of electronic charge still stays in donor pyridine (phenyl) rings.

The molecules PZ3 and AZ3 represent an octupolar system, where electrons are free to move in all six directions depending upon the electron-accepting/donating characters of moieties included in the molecule. In AZ3, the electron density is majorly concentrated on the first and second arms of molecules in HOMO. Upon electronic excitation, the electronic charge gets shifted to the triazine core and third arm, while a moderate amount of electronic charge stays in the second arm. In PZ3, a major amount of electron density is found in the first and second arms of a molecule in HOMO. In LUMO of PZ3, electronic charge moves to third arm and central triazine core completely so that first and second arms are almost devoid of charges.

3.6. First hyperpolarizability

Organic molecules are gaining importance in non-linear optics as they exhibit good NLO activity because of, a) convenience of electron movement across a molecule due to delocalizable π -electrons, b) extendable π -conjugation, which provides a path for electron movement, c) crystallization of a molecule in a non-centrosymmetric crystal lattice, which encourages an increase in optical nonlinearity [74,75], d) ease of functionalization of a donor and an acceptor at the terminals of the conjugated molecular system, which induces charge asymmetry and gives rise to charge transfer within the molecule. Hence, we proceeded to calculate the first order non-linearity (first hyperpolarizability) of molecules under study.

The total first hyperpolarizabilities (β) of all the molecules under study calculated at B3LYP/6-31G (d, p) level of theory are presented in Table 5. All the molecules (except PZ1 and AZ1) showed β values of the order of 10^{-29} esu, which is comparable to that of standard molecule p-nitroaniline (PNA) having β value of 1.28×10^{-29} esu [76].

One can observe from Table 5 that, nucleophilic substitution pattern has altered the non-linearity of molecules in such a way that; the order of β in PZ series is PZ3 > PZ2 > PZ1 and that in AZ series is AZ3 > AZ2 >

Table 5

The total first hyperpolarizabilities ($\beta \times 10^{-29}$ esu) of all the molecules under study calculated at B3LYP/6-31G (d, p) level of theory.

Name	AZ1	AZ2	AZ3	PZ1	PZ2	PZ3	PNA
β	1.17	1.57	2.04	0.95	1.51	1.85	1.28 ^a

^a Reference number [76].

AZ1. The increasing conjugation length as we proceed from mono- to di- to tri-substituted triazine has prompted the β value to increase in the same order.

It is known that good electron donors promote the first hyperpolarizability of a molecule. Hence, the β of PZ series molecules (having electron-donating pyridine moieties) is higher than that of their counterparts in AZ series.

3.7. Electron affinity and ionization potential

The competent injection of hole and electron into an organic system has a greater impact on the applicability of that system as an optoelectronic device. The factors like electron affinity (EA) and ionization potential (IP) of a molecule highly influence the threshold of energy for the injection of holes and electrons into that molecule. The electron affinities and ionization potentials of all the molecules under investigation, which are calculated at B3LYP/6-31G (d, p) level of theory are shown in Table 6.

EA is the energy unleashed when an electron is added to the system. Higher values of EA facilitate competent electron injection into LUMO of a molecule. When a molecule has high EA; it will be very easy to inject electrons from cathode to electron-transport layer (ETL) material made of that particular molecule. In PZ series of molecules, the order of EA is as follows: PZ3 > PZ2 > PZ1. Hence, as the nucleophilic substitution increases the EA is also increasing. Reverse the order of EA (AZ3 < AZ2 < AZ1) is followed in the case of AZ series of molecules.

The EA of PZ series of molecules is higher than their counterparts in AZ series. Perhaps, this is because of the observation that the LUMO energies of molecules in PZ series are lower as compared to their counterparts in AZ series molecules and hence the addition of an electron to LUMO's of PZ series molecules is easier as compared to those of AZ series molecules.

IP is the energy supplied to the system to expel an electron from its outermost orbital. Lower magnitudes of IP promote the efficient injection of the hole into the HOMO of the molecule. Hence it will be easier to induce hole into the hole-transport layer (HTL) of molecules having lower IPs from indium tin oxide (ITO).

In PZ series of molecules IP remains negligibly affected by increasing substitution from PZ1 to PZ3. But in the case of AZ series of molecules, AZ3 shows the lowest IP as compared to AZ1 and AZ2. When we compare IPs of AZ and PZ series, we see that PZ series molecules show lower IPs than those of AZ series molecules.

3.8. Reorganization energy

Reorganization energy (λ) indicates the energy change of the system upon molecular structure relaxation due to the surplus number of positive and negative charges. λ values assist in the assessment of the rate of charge transportation. Lower the λ value; better will be the charge-transport rate (Eqs. (3) and (4)) and higher will be the prospectus of application of those molecules in the construction of OLEDs. The B3LYP/6-31G (d, p) method calculated reorganization energies (both λ_h and λ_e) of all the molecules are given in Table 6.

In PZ series of molecules, as the nucleophilic substitution increases from PZ1 to PZ3; the λ_h values are decreasing. It means that hole reorganization energies are improving with the addition of each pyridine

Table 6

The electron affinities (EA in meV), ionization potentials (IP in meV), hole reorganization energies (λ_h in meV) and electron reorganization energies (λ_e in meV) of all the molecules under study computed at B3LYP/6-31G (d, p) method.

Name	EA	IP	λ_h	λ_e
AZ1	0.36	7.86	477	1734
AZ2	-0.18	7.28	188	516
AZ3	-0.48	6.82	81	344
PZ1	2.10	5.53	448	1517
PZ2	2.13	5.52	160	348
PZ3	2.22	5.66	133	258

moiety with a nitrogen bridge from PZ1 to PZ3. Both PZ2 and PZ3 show better λ_h values (160 meV and 133 meV respectively) as compared to the standard hole transport material *N,N'*-diphenyl-*N,N'*-bis(3-methylphenyl)-(1,1'-biphenyl)-4,4'-diamine (TPD), which shows $\lambda_h = 290$ meV [77]. The same trend is followed in AZ series also, where AZ2 and AZ3 exhibit improved λ_h values (188 meV and 81 meV respectively) as compared to TPD.

The comparison of λ_h values of AZ and PZ series of molecules show that phenyl substituted AZ3 is the best hole transport material ($\lambda_h = 81$ meV) as compared to pyridine substituted PZ3 ($\lambda_h = 133$ meV). AZ1 and AZ2 show approximately the same values of λ_h as those of PZ1 and PZ2.

The λ_e values of both PZ and AZ series of molecules are not encouraging (except PZ3) since their electron-transporting rates fall below than that of tris(8-hydroxyquinolino)aluminium(III) (Alq₃, $\lambda_e = 276$ meV) [78]. Only PZ3 shows good λ_e value (=258 meV) as compared to standard material Alq₃.

4. Conclusions

The combined experimental and computational studies presented in this work aimed at the design and synthesis of some triazine molecules in order to discover the influence of increasing nucleophilic substitution (on central triazine core) and incorporation of a hetero (nitrogen) atom (in the electron-donating wings of triazines) on the linear and non-linear optical properties as well as reorganization energies of molecules. The main findings emerged from this study are: 1) The molecule PZ2 shows experimental absorbance and λ_{exp} almost equal to those of AZ3 (which is already patented as a component in sunscreen compositions) and can be probed for used in sunscreen components, 2) The absorption spectrum of each molecule is characterized by the presence of very intense $\pi \rightarrow \pi^*$ electronic transition in absorption system I and four $n \rightarrow \pi^*$ electronic transitions (one allowed and three forbidden) in absorption system II, 3) TD-DFT calculations indicate the blue-shifting of highly intense λ_{cal} of molecules with increasing nucleophilic substitution on triazine core, 4) The molecules AZ2, AZ3, PZ2 and PZ3 show better hole reorganization energies than the standard material TPD ($\lambda_h = 290$ meV), 5) Among all molecules in AZ and PZ series; AZ3 shows least hole reorganization energy ($\lambda_h = 81$ meV), which indicates AZ3 is the best hole transporting material among all molecules though AZ2, PZ2 and PZ3 also show good hole transporting abilities, 6) All the molecules except AZ1 and PZ1 show good magnitudes of first hyperpolarizabilities comparable to PNA and can be prospective candidates in NLO applications.

CRediT authorship contribution statement

V.M. Vidya: Methodology, Investigation, Formal analysis, Writing - original draft. **Someshwar Pola:** Methodology, Formal analysis. **Chetti Prabhakar:** Conceptualization, Software, Validation, Formal analysis, Resources, Writing - review & editing, Supervision, Project administration.

Declaration of competing interest

The authors declare that they have no known competing financial interests or personal relationships that could have appeared to influence the work reported in this paper.

Acknowledgments

Authors thank to CSIR New Delhi, India [02(0339)/18/EMR-II] and DST, New Delhi, India (WOS-A scheme, SR/WOS-A/CS-46/2017) for financial support. Authors thank GJU, Hisar and SAIF, Chandigarh for providing NMR facilities and IIT, Ropar for providing mass spectra measurement facilities. The authors are thankful to Dr. Avijit Kumar

Paul for single crystal data measurements. The authors are also thankful to Dr. L. Giribabu, CSIR-IIT for supporting in CV data.

Appendix A. Supplementary data

Supplementary data to this article can be found online at <https://doi.org/10.1016/j.saa.2020.118940>.

References

- [1] F. Zhou, I. Abdelwahab, K. Leng, K.P. Loh, W. Ji, 2D perovskites with giant excitonic optical nonlinearities for high-performance sub-bandgap photodetection, *Adv. Mater.* 31 (2019) 1904155, <https://doi.org/10.1002/adma.201904155>.
- [2] Y.Y. Li, W.J. Wang, H. Wang, H. Lin, L.M. Wu, Mixed-anion inorganic compounds: a favorable candidate for infrared nonlinear optical materials, *Cryst. Growth Des.* 19 (2019) 4172–4192, <https://doi.org/10.1021/acs.cgd.9b00358>.
- [3] Y. Zhang, Y. Long, X. Dong, L. Wang, L. Huang, H. Zeng, Z. Lin, X. Wang, G. Zou, Y80 (OH)15(CO3)3Cl: an excellent short-wave UV non-linear optical material exhibiting an infrequent three-dimensional inorganic cationic framework, *Chem Commun* 55 (2019) 4538–4541, <https://doi.org/10.1039/c9cc00581a>.
- [4] O. Ostroverkhova, Organic optoelectronic materials: mechanisms and applications, *Chem. Rev.* 116 (2016) 13279–13412, <https://doi.org/10.1021/acs.chemrev.6b00127>.
- [5] J. Balaji, P. Srinivasan, S. Prabu, M. George, D. Sajan, Growth and dielectric studies of toluidine tartrate single crystals: a novel organic NLO material, *J. Mol. Struct.* 1207 (2020) 127750, <https://doi.org/10.1016/j.molstruc.2020.127750>.
- [6] S.I. Kim, W.T. Kim, J.H. Seok, M. Jazbinsek, W. Yoon, I.C. Yu, H. Yun, D. Kim, F. Rotermond, O.P. Kwon, Organic σ -hole containing crystals with enhanced nonlinear optical response and efficient optical-to-THz frequency conversion, *Adv Opt Mater* (2020) <https://doi.org/10.1002/adom.201901840> (Ahead of print).
- [7] Sas E. Babur, Characterization, optical and nonlinear optical properties of TAZ organic material, *Optik* 188 (2019) 91–98, <https://doi.org/10.1016/j.ijleo.2019.04.049>.
- [8] C.N. Ironside, Nonlinear optical devices, in: R.W. Munn, C.N. Ironside (Eds.), *Principles and Applications of Nonlinear Optical Materials*, Springer Science+Business Media, Dordrecht 1993, pp. 20–33.
- [9] A. Lorente, P. Pingel, G. Liaptsis, H. Krueger, S. Janietz, Modulation of ambipolar charge transport characteristics in side-chain polystyrenes as host materials for solution processed OLEDs, *Org. Electron.* 41 (2017) 91–99, <https://doi.org/10.1016/j.orgel.2016.11.036>.
- [10] R. Jin, Theoretical study of the optical and charge transport properties of star-shaped molecules with 1,3,5-triazine-core derivatives as organic light-emitting and organic solar cells materials, *CR Chim* 18 (2015) 954–959, <https://doi.org/10.1016/j.crci.2015.05.021>.
- [11] V. Vaitkeviciene, J.V. Grazulevicius, V. Pecuriate, S. Grigalevicius, V. Jankauskas, Triazine-based aromatic amines as new glass-forming charge transport materials, *Mol. Cryst. Liq. Cryst.* 468 (2007) 493–502, <https://doi.org/10.1080/15421400701229776>.
- [12] N. Zhang, Q.L. Guan, C.H. Liu, Y. Sun, B. Li, Y.H. Xing, F.Y. Bai, Arht-type luminescent Zn (II)-MOF constructed by triazine hexacarboxylate ligand: tunable luminescent performance and white-light emission regulation through doping $\text{Eu}^{3+}/\text{Tb}^{3+}$, *Appl. Organomet. Chem.* 34 (2020), e5506, <https://doi.org/10.1002/aoc.5506>.
- [13] G. Zhao, D. Liu, W. Tian, W. Jiang, Y. Sun, Rational molecular design of novel host material combing intra- and intermolecular charge transfers for efficient solution-processed organic light-emitting diodes, *Dyes Pigments* 175 (2020) 108188, <https://doi.org/10.1016/j.dyepig.2020.108188>.
- [14] Y. Wang, Y. Wang, G. Wang, D. Liu, Ultrafast pump-probe and time-resolved fluorescence anisotropy study of the intramolecular interaction of branched styryl derivatives based on 1,3,5-triazine, *J Nonlinear Opt Phys* 28 (2019) 1950003, <https://doi.org/10.1142/s0218863519500036>.
- [15] B. Liu, H. Wang, Q. Hu, Hyper-Rayleigh scattering studies of a three-photon fluorescent non-linear optical molecule at 1500 nm, *Chem. Phys. Lett.* 716 (2019) 252–256, <https://doi.org/10.1016/j.cplett.2018.11.059>.
- [16] A. Jimenez-Sanchez, I. Isunza-Manrique, G. Ramos-Ortiz, J. Rodriguez-Romero, N. Farfan, R. Santillan, Strong dipolar effects on an octupolar luminescent chromophore: implications on their linear and nonlinear optical properties, *J. Phys. Chem. A* 120 (2016) 4314–4324, <https://doi.org/10.1021/acs.jpca.6b02805>.
- [17] Q. Liu, X. Zhao, F. Zhou, Y.L. Song, W.H. Zhang, J.P. Lang, Assembly of [Tp*WS3Cu2]-supported coordination polymers from linkers with a unique μ -pyridyl bridging mode and their enhanced third-order nonlinear optical performances, *Cryst. Growth Des.* 16 (2016) 3206–3214, <https://doi.org/10.1021/acs.cgd.6b00115>.
- [18] K.P. Subodh, K. Chaudhary, D.T. Masram, A new triazine-cored covalent organic polymer for catalytic applications, *Appl. Catal. A Gen.* 593 (2020) 117411, <https://doi.org/10.1016/j.apcata.2020.117411>.
- [19] G. Li, X. Zhou, Z. Wang, Highly nitrogen-rich microporous polyaminals using *N,N*-dimethylformamide and formamide as the starting monomers for CO₂ adsorption and separation, *J. Phys. Chem. C* 124 (2020) 3087–3094, <https://doi.org/10.1021/acs.jpcc.9b10590>.
- [20] Y.J. Ma, J.X. Hu, S.D. Han, J. Pan, J.H. Li, G.M. Wang, Manipulating on/off single-molecule magnet behavior in a Dy(III)-based photochromic complex, *J. Am. Chem. Soc.* 142 (2020) 2682–2689, <https://doi.org/10.1021/jacs.9b13461>.
- [21] J. Zhang, T. Zheng, J. Zhang, I₂/K₂S₂O₈ mediated direct oxidative annulation of alkylazaarenes with amidines for the synthesis of substituted 1,3,5-triazines, *Eur. J. Org. Chem.* 2020 (2020) 860–865, <https://doi.org/10.1002/ejoc.201901737>.

- [22] B. Niu, S. Li, C. Cui, Y. Yan, L. Tang, J. Wang, New strategy for the synthesis of heterocycles via copper-catalyzed oxidative decarboxylative amination of glyoxylic acid, *Eur. J. Org. Chem.* 48 (2019) 7800–7803, <https://doi.org/10.1002/ejoc.201901538>.
- [23] W. Guo, M. Zhao, C. Du, L. Zheng, L. Li, L. Chen, K. Tao, W. Tan, Z. Xie, L. Cai, X. Fan, K. Zhang, Visible-light-catalyzed [3 + 1 + 2] coupling annulations for the synthesis of unsymmetrical tri-substituted amino-1,3,5-triazines, *J. Org. Chem.* 84 (2019) 15508–15519, <https://doi.org/10.1021/acs.joc.9b02514>.
- [24] Y. Zhang, Y. Liu, J. Zhang, R. Gu, S. Han, An alternatively metal-free synthesis of 1,3,5-triazines 1,2,4-thiadiazoles from benzyl chlorides and benzylamines mediated by elemental sulfur, *Tetrahedron Lett.* 60 (2019) 151289, <https://doi.org/10.1016/j.tetlet.2019.151289>.
- [25] Y. Yan, C. Cui, J. Wang, S. Li, L. Tang, Y. Liu, Transition metal-free C-F/C-Cl/C-C cleavage of ClCF₂COONa for the synthesis of heterocycles, *Org. Biomol. Chem.* 17 (2019) 8071–8074, <https://doi.org/10.1039/c9ob01641d>.
- [26] Z. Yan, Y. Li, M. Ma, Solvent-directed click reaction between active methylene compounds and azido-1,3,5-triazines, *Org. Lett.* 21 (2019) 7204–7208, <https://doi.org/10.1021/acs.orglett.9b02089>.
- [27] X. Yu, Ma X. Zhou, Y. Q. Song, Transition metal-free assembly of 1,3,5-triazines using ethyl bromodifluoroacetate as C1 source, *Chem. Commun.* 55 (2019) 8079–8082, <https://doi.org/10.1039/c9cc03534f>.
- [28] M.J. Frisch, G.W. Trucks, H.B. Schlegel, G.E. Scuseria, M.A. Robb, J.R. Cheeseman, G. Scalmani, V. Barone, G.A. Petersson, H. Nakatsuji, X. Li, M. Caricato, A.V. Marenich, J. Bloino, B.G. Janesko, R. Gomperts, B. Mennucci, H.P. Hratchian, J.V. Ortiz, A.F. Izmaylov, J.L. Sonnenberg, D. Williams-Young, F. Ding, F. Lipparini, F. Egidi, J. Goings, B. Peng, A. Petrone, T. Henderson, D. Ranasinghe, V.G. Zakrzewski, J. Gao, N. Rega, G. Zheng, W. Liang, M. Hada, M. Ehara, K. Toyota, R. Fukuda, J. Hasegawa, M. Ishida, T. Nakajima, Y. Honda, O. Kitao, H. Nakai, T. Vreven, K. Throssell, M. Ishigomori, J.A. Peralta, F. Ogliaro, M.J. Bearpark, J.J. Heyd, E.N. Brothers, K.N. Kudin, V.N. Staroverov, T.A. Keith, R. Kobayashi, J. Normand, K. Raghavachari, A.P. Rendell, J.C. Burant, S.S. Iyengar, J. Tomasi, M. Cossi, J.M. Millam, M. Klene, C. Adamo, R. Cammi, J.W. Ochterski, R.L. Martin, K. Morokuma, O. Farkas, J.B. Foresman, D.J. Fox, Gaussian 16, Revision B.01, Gaussian, Inc., Wallingford CT, 2016.
- [29] A.D. Becke, Density-functional exchange-energy approximation with correct asymptotic behavior, *Phys. Rev. A* 38 (1988) 3098–3100, <https://doi.org/10.1103/PhysRevA.38.3098>.
- [30] C. Lee, W. Yang, R.G. Parr, Development of the Colle-Salvetti correlation-energy formula into functional of the electron density, *Phys. Rev. B* 37 (1988) 785–789, <https://doi.org/10.1103/PhysRevB.37.785>.
- [31] Bredas JL, Meyers F, Pierce BM, Zyss J. On the second-order polarizability of conjugated π -electron molecules with octupolar symmetry: the case of triaminotrirobenzene. *J Am Chem Soc* 992;114:4928–4929. DOI:<https://doi.org/10.1021/ja00038a082>.
- [32] D.R. Kanis, M.A. Ratner, T.J. Marks, Design and construction of molecular assemblies with large second-order optical nonlinearities. Quantum chemical aspects, *Chem. Rev.* 94 (1994) 195–242, <https://doi.org/10.1021/cr00025a007>.
- [33] V.M. Vidya, C. Prabhakar, A DFT probe on the linear and nonlinear optical characteristics of some star-shaped DI- π -DII-A type acetylene-bridged rigid triazines, *J. Phys. Org. Chem.* 33 (2020) 4027, <https://doi.org/10.1002/poc.4027>.
- [34] R.A. Marcus, Electron transfer reactions in chemistry, Theory and experiment. *Rev Mod Phys* 65 (1993) 599–610, <https://doi.org/10.1103/RevModPhys.65.599>.
- [35] R.A. Marcus, H. Eyring, Chemical and electrochemical electron-transfer theory, *Annu Rev Phys Chem* 15 (1964) 155–196, <https://doi.org/10.1146/annurev.pc.15.100164.001103>.
- [36] D.P. McMahon, A. Troisi, Evaluation of the external reorganization energy of polycenes, *J. Phys. Chem. Lett.* 1 (2010) 941–946, <https://doi.org/10.1021/jz1001049>.
- [37] K. Srinivas, S. Sitha, V.J. Rao, K. Bhanuprakash, K. Ravikumar, S.P. Anthony, T.P. Radhakrishnan, First hyperpolarizability of some nonconjugated donor–acceptor 3D molecules: noncentrosymmetric crystal through conformational flexibility, *J. Mater. Chem.* 15 (2005) 965–973, <https://doi.org/10.1039/b414311f>.
- [38] E. Halay, Y. Acikbas, R. Capan, S. Bozkurt, M. Erdogan, R. Unal, A novel triazine-bearing calix[4]arene: design, synthesis and gas sensing affinity for volatile organic compounds, *Tetrahedron* 75 (2019) 2521–2528, <https://doi.org/10.1016/j.tet.2019.03.027>.
- [39] S.M. Osman, S.N. Khattab, E.S.A. Aly, E.R. Kenawy, A. El-Faham, 1,3,5-Triazine-based polymer: synthesis, characterization and application for immobilization of silver nanoparticles, *J. Polym. Res.* 24 (2017) 1–13, <https://doi.org/10.1007/s10965-017-1385-2>.
- [40] M. Dinari, F. Gharahi, P. Asadi, Synthesis, spectroscopic characterization, antimicrobial evaluation and molecular docking study of novel triazine-quinazolinone based hybrids, *J. Mol. Struct.* 1156 (2018) 43–50, <https://doi.org/10.1016/j.molstruc.2017.11.087>.
- [41] X. Wang, Y. Xu, L. Yang, X. Lu, H. Zou, W. Yang, Y. Zhang, Z. Li, M. Ma, Synthesis, spectra, and theoretical investigations of 1,3,5-triazine compounds as ultraviolet rays absorber based on time-dependent density functional calculations and three-dimensional quantitative structure–property relationship, *J. Fluoresc.* 28 (2018) 707–723, <https://doi.org/10.1007/s10895-018-2235-2>.
- [42] K.A. Kolmakov, An efficient, “green” approach to aryl amination of cyanuric chloride using acetic acid as solvent, *J. Heterocycl. Chem.* 45 (2008) 533–539, <https://doi.org/10.1002/jhet.5570450236>.
- [43] J.T. Thurston, J.R. Dudley, D.W. Kaiser, I. Hechenbleikner, F.C. Schaefer, D. Holm-Hansen, Cyanuric acid derivatives. I. Aminochloro-s-triazines, *J. Am. Chem. Soc.* 73 (1951) 2981–2983, <https://doi.org/10.1021/ja01151a001>.
- [44] K. Arya, A. Dandia, Synthesis and cytotoxic activity of trisubstituted-1,3,5-triazines, *Bioorg. Med. Chem. Lett.* 17 (2007) 3298–3304, <https://doi.org/10.1016/j.bmcl.2007.04.007>.
- [45] O. Shemchuk, D. Braga, F. Grepioni, R.J. Turner, Co-crystallization of antibacterials with inorganic salts: paving the way to activity enhancement, *RSC Adv.* 10 (2020) 21466–2149, <https://doi.org/10.1039/c9ra10353h>.
- [46] L. Mazzei, V. Broll, L. Casali, M. Silva, D. Braga, F. Grepioni, J. Baltrusaitis, S. Ciurli, Multifunctional urea cocrystal with combined ureolysis and nitrification inhibiting capabilities for enhanced nitrogen management, *ACS Sustain. Chem. Eng.* 7 (2019) 13369–13378, <https://doi.org/10.1021/acsuschemeng.9b02607>.
- [47] SMART, (V 5.628), SAINT (V 6.45a), XPREP, SHELXTL, Bruker AXS Inc, Madison, Wisconsin, USA, 2004.
- [48] G.M. Sheldrick, Siemens Area Detector Absorption Correction Program, University of Göttingen, Göttingen, Germany, 1994.
- [49] G.M. Sheldrick, SHELXL-97 Program for Crystal Structure Solution and Refinement, University of Göttingen, Göttingen, Germany, 1997.
- [50] J.L. Farrugia, WinGX suite for small-molecule single-crystal crystallography, *J. Appl. Crystallogr.* 32 (1999) 837–838, <https://doi.org/10.1107/S0021889899006020>.
- [51] A.L. Spek, PLATON SQUEEZE: a tool for the calculation of the disordered solvent contribution to the calculated structure factors, *Acta Crystallogr. Sect. C Struct. Chem.* 71 (2015) 9–18, <https://doi.org/10.1107/S2053229614024929>.
- [52] T. Zeng, C.M. Dong, X.G. Shu, N-(4,6-Dichloro-1,3,5-triazin-2-yl)aniline, *Acta Crystallogr. A* 61 (2005) o2334–o2335, <https://doi.org/10.1107/S1600536805020386>.
- [53] R.C. Hirt, D.J. Salley, Ultraviolet absorption spectra of derivatives of symmetric triazine, I. Amino Triazines, *J. Chem. Phys.* 21 (1953) 1181–1184, <https://doi.org/10.1063/1.1699160>.
- [54] L. Goodman, $n \rightarrow \pi^*$ transitions in the azines, *J. Mol. Spectrosc.* 6 (1961) 109–137, [https://doi.org/10.1016/0022-2852\(61\)90235-1](https://doi.org/10.1016/0022-2852(61)90235-1).
- [55] J.S. Brinen, L. Goodman, Low resolution analysis of the $n \rightarrow \pi^*$ (3000 Å) absorption spectrum of s-triazine, *J. Chem. Phys.* 35 (1961) 1219–1225, <https://doi.org/10.1063/1.1732026>.
- [56] R.C. Hirt, F. Halverson, R.G. Schmitt, s-Triazine. II. The near ultraviolet absorption spectrum, *J. Chem. Phys.* 22 (1954) 1148–1149, <https://doi.org/10.1063/1.1740306>.
- [57] F. Halverson, R.C. Hirt, Near ultraviolet solution spectra of the diazines, *J. Chem. Phys.* 19 (1951) 711–718, <https://doi.org/10.1063/1.1748338>.
- [58] G.J. Brealey, M. Kasha, The role of hydrogen bonding in the $n \rightarrow \pi^*$ blue-shift phenomenon, *J. Am. Chem. Soc.* 77 (1955) 4462–4468, <https://doi.org/10.1021/ja01622a006>.
- [59] K.K. Innes, J.A. Merritt, W.C. Tincher, S.G. Tilford, Ultra-violet absorption spectra of the diazines, *Nature* 187 (1960) 500–501, <https://doi.org/10.1038/187500a0>.
- [60] C.G. Overberger, S.L. Shapiro, The ultraviolet absorption spectra of substituted aminotriazines, *J. Am. Chem. Soc.* 76 (1954) 1855–1858, <https://doi.org/10.1021/ja01636a035>.
- [61] R.R. Renji, V.G. Juozas, S. Jurate, M. Tomas, M. Arunas, K. Karolis, J. Saulius, D. Przemyslaw, L. Mieczyslaw, Z. Pawel, Glass forming donor-substituted s-triazines: photophysical and electrochemical properties, *Dyes Pigments* 97 (2013) 412–422, <https://doi.org/10.1016/j.dyepig.2013.01.017>.
- [62] R. Fink, C. Frenz, M. Thelakkat, H.W. Schmidt, Synthesis and characterization of aromatic poly(1,3,5-triazine-ether)s for electroluminescent devices, *Macromolecules* 30 (1997) 8177–8181, <https://doi.org/10.1021/ma970528x>.
- [63] Heischkel Y. Fink, M. Thelakkat, H.W. Schmidt, C. Jonda, M. Huppauß, Synthesis and application of dimeric 1,3,5-triazine ethers as hole-blocking materials in electroluminescent devices, *Chem. Mater.* 10 (1998) 3620–3625, <https://doi.org/10.1021/cm980369b>.
- [64] Y. Tan, Z. Zhao, L. Shang, Y. Liu, C. Wei, J. Li, H. Wei, Z. Liu, Z. Bian, C. Huang, A novel bipolar D- π -A type phenanthroimidazole/carbazole hybrid material for high efficiency nonpopped deep-blue organic light-emitting diodes with NTSC CIE: Y and low efficiency roll-off, *J. Mater. Chem. C* 5 (2017) 11901–11909, <https://doi.org/10.1039/c7tc04089j>.
- [65] C.G.L. Maria, M.M.F. Blanca, C.N. Rodrigo, M.J.P. Victor, M. Ivana, A. Eduardo, R.O. Alejandro, E.O. Maria, Microwave-assisted synthesis, third-order nonlinear optical properties, voltammetry cyclic and theoretical calculations of organotin compounds bearing push-pull Schiff bases, *J. Organomet. Chem.* 806 (2016) 68–76, <https://doi.org/10.1016/j.jorganchem.2016.01.030>.
- [66] L. Fotouhi, N. Farzinnegad, M.M. Heravi, Sh. Khaleghi, Study the electrochemical reduction of some triazines in N,N-dimethylformamide at glassy carbon electrode, *Bull. Kor. Chem. Soc.* 24 (2003) 1751–1756, <https://doi.org/10.5012/bkcs.2003.24.12.1751>.
- [67] J.M. Saveant, *Elements of Molecular and Biomolecular Electrochemistry: An Electrochemical Approach to Electron Transfer Chemistry*, First ed. John Wiley & Sons, Paris, 2006 455.
- [68] J.L. Bredas, Mind the gap! *Mater. Horiz* 1 (2014) 17–19, <https://doi.org/10.1039/c3mh00098b>.
- [69] X. Li, H. Huang, H. Bin, Z. Peng, C. Zhu, L. Xue, Z.G. Zhang, Z. Zhang, H. Ade, Y. Li, Synthesis and photovoltaic properties of a series of narrow bandgap organic semiconductor acceptors with their absorption edge reaching 900 nm, *Chem. Mater.* 29 (2017) 10130–10138, <https://doi.org/10.1021/acs.chemmater.7b03928>.
- [70] J.C.S. Costa, R.J.S. Taveira, C.F.R.A.C. Lima, A. Mendes, L.M.N.B.F. Santos, Optical band gaps of organic semiconductor materials, *Opt. Mater.* 58 (2016) 51–60, <https://doi.org/10.1016/j.optmat.2016.03.041>.
- [71] K.J. Hamam, M.I. Alomari, A study of the optical band gap of zinc phthalocyanine nanoparticles using UV–Vis spectroscopy and DFT function, *Appl. Nanosci.* 7 (2017) 261–268, <https://doi.org/10.1007/s13204-017-0568-9>.
- [72] X. Liu, Y. Sun, B.B.Y. Hsu, A. Lorbach, L. Qi, A.J. Heeger, G.C. Bazan, Design and properties of intermediate-sized narrow band-gap conjugated molecules relevant to solution-processed organic solar cells, *J. Am. Chem. Soc.* 136 (2014) 5697–5708, <https://doi.org/10.1021/ja413144u>.
- [73] S.Z. Topal, U. Isci, U. Kumru, D. Atilla, A.G. Guerek, C. Hirel, M. Durmus, J.B. Tommasino, D. Luneau, S. Berber, F. Dumoulin, V. Ahseen, Modulation of the

- electronic and spectroscopic properties of Zn(II) phthalocyanines by their substitution pattern, Dalton Trans. 43 (2014) 6897–6908, <https://doi.org/10.1039/c3dt53410c>.
- [74] D.S. Chemla, J. Zyss, *Nonlinear Optical Properties of Organic Molecules and Crystals*, Academic Press, New York, 1987.
- [75] Ch. Bosshard, R. Spreiter, M. Zgonik, P. Günter, Kerr nonlinearity via cascaded optical rectification and the linear electro-optic effect, Phys. Rev. Lett. 74 (1995) 2816–2819, <https://doi.org/10.1103/PhysRevLett.74.2816>.
- [76] C.C. Teng, A.F. Garito, Dispersion of the nonlinear second-order optical susceptibility of organic systems, Phys. Rev. B 28 (1983) 6766–6773, <https://doi.org/10.1103/PhysRevB.28.6766>.
- [77] M. Malagoli, J.L. Bredas, Density functional theory study of the geometric structure and energetics of triphenylamine-based hole-transporting molecules, Chem. Phys. Lett. 327 (2000) 13–17, [https://doi.org/10.1016/S0009-2614\(00\)00757-0](https://doi.org/10.1016/S0009-2614(00)00757-0).
- [78] B.C. Lin, C.P. Cheng, Z.Q. You, C.P. Hsu, Charge transport properties of tris(8-hydroxyquinolato)aluminum(III): why it is an electron transporter, J. Am. Chem. Soc. 127 (2005) 66–67, <https://doi.org/10.1021/ja045087t>.